

# Efficient Optimization-based Cable Force Allocation for Geometric Control of Multiple Quadrotors Transporting a Payload

Khaled Wahba and Wolfgang Hönig

**Abstract**—We consider transporting a heavy payload that is attached to multiple quadrotors. The current state-of-the-art controllers either do not avoid inter-robot collision at all, leading to crashes when tasked with carrying payloads that are small in size compared to the cable lengths, or use computational demanding nonlinear optimization. We propose an extension to an existing efficient geometric payload transport controller to effectively avoid such collisions by designing an optimized cable force allocation method, and thus retaining the original stability properties. Our approach introduces a cascade of carefully designed quadratic programs that can be solved efficiently on highly constrained embedded flight controllers.

We demonstrate our method on challenging scenarios with up to three small quadrotors with various payloads and cable lengths, with our controller running in real-time directly on the robots.

## I. INTRODUCTION

Aerial vehicles can operate in places that are hard to reach by other robots. As such, they are well suited for collaborative assistance in a construction site, removal of rubble in a search-and-rescue scenario, or decommissioning of a nuclear power plant. Cable-driven payload transportation using multi-UAVs is beneficial because it does not require carrying manipulators or grippers onboard the quadrotors, thus allowing to transport heavier objects [16], which makes them in particular interesting for transporting tools or supplies [5].

State-of-the-art controllers for a team of multirotors to transport a cable-suspended payload include geometric controllers [8, 10] as well as nonlinear model predictive control [24]. These existing works either ignore possible collisions between robots [8], or use a nonlinear optimization framework that necessitates complex on-board computation [13, 24]. Collision between robots can easily occur for payloads that are small in size compared to the robot's size and the cable length which poses a safety risk.

We propose a new cable force allocation method for the geometric controller by Lee [8] that provides the team with new capabilities, see Fig. 1. In particular we directly consider safety distances between robots and allow for user-preferred formations. Our formulation uses a cascaded design of three low-dimensional quadratic programs (QPs), which have global minima that can be found within milliseconds even on highly resource-limited microcontrollers. In fact, this approach allows us to execute the control law in a distributed fashion on physical robots. Effectively, our method allows users to teleoperate a team of robots by simply commanding the payload, independent of the payload size.

In particular, our contributions are as follows:

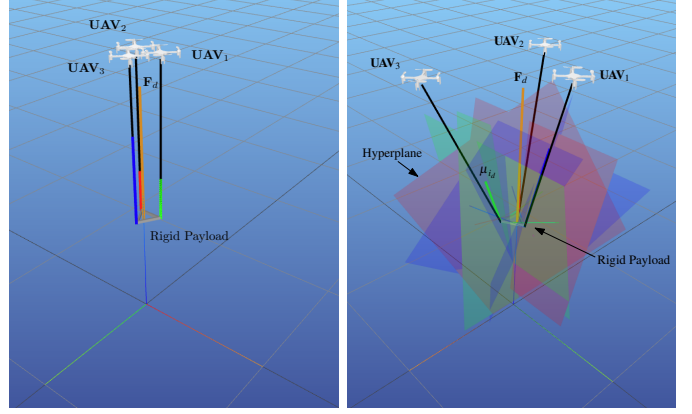


Fig. 1. Three quadrotors carrying a payload. Left: The baseline controller [8] allocates the desired cable forces with the minimum-norm solution, causing inter-robot collisions. Right: Our contribution of an efficient and effective approach to compute the desired cable forces, such that collisions between robots are avoided. To this end, we compute hyperplanes that define a safe convex set for the desired cable forces, while considering the desired motion of the payload.

- 1) Algorithmically, we provide a new QP-based force allocation method that can be deployed on highly constrained microcontrollers.
- 2) Empirically, we evaluate the baseline by Lee [8] and our method on a team of up to three small (30 g) quadrotors where the controller runs in a distributed fashion on-board.

We note that while the geometric controller has been shown very recently (concurrently to our work) on a team of larger (250 g) physical multirotors [11, 13], we are the first to bring this capability to a highly constrained flight controller.

## II. RELATED WORK

The dynamics of the cable-suspended payload system with multi-UAVs can be described explicitly through the interaction forces between the payload, cables, and the UAVs [16]. In general, the dynamics are expressed using Newton's equations of motion [19, 26, 27], while augmenting the rotational dynamics of the UAVs [8].

There has been some advancement towards control algorithms for payload collaborative transport. A Leader-Follower paradigm has been proposed in several works [25, 26]. These methods use the interaction forces between the robots and the payload-cable system to ensure that the follower robot would be compliant with the leader. While these methods do not require any communication between the UAVs, the dependency on the leader poses a risk in case of its failure.

Other methods depend on constructing a cascaded design for the control law using either force [8, 26] or kinematic analysis [22]. In particular, the authors in [8, 10] introduced a geometric cascaded controller on  $SE(3)$  for cable-driven payload transportation using multi-UAVs. The cascaded design enables the computation of the control input of each UAV given a reference trajectory for the payload. The exponential stability of the controlled full dynamics is shown through Lyapunov analysis. However, the cascaded structure imposes challenges in practice. The method requires either the measurement or estimation of the accelerations of the payload, which is impractical due to the induced noise. Moreover, the controller is not designed to avoid robot/robot collision or cable tangling.

Offline motion planners [15] are also considered in providing high-level references to the cascaded designs. Here, the planner takes into account the position of each quadrotor to achieve a desired start to goal motion for the payload. Another high-level formation control planner [2] is augmented with the cascaded designs to take into account inter-robot collisions and configure the quadrotors into desired formations. However, both methods do not reason over the force allocation or load distribution of the quadrotors. Thus, they might propose configurations for the team where the load distribution is unfeasible, or present slackness in the cables which is not modeled in both methods.

Methods to avoid inter-robot collision and impose safety constraints include a null-space method with a closed-form solution [13] and a nonlinear optimization formulation [12, 13]. The former cannot impose a predefined safety distance between UAVs, as it only maximizes the minimum distances between the robots. While the latter suffers from the requirement of a good initial guess as well as slow computation. The authors of [13] provide real physical experiments of the two methods in a safety-awareness context as well as a simulator [11] with an open-source implementation of one the controllers.

Nonlinear optimization is also considered to tackle the full control problem [24]. In particular, nonlinear model predictive control (NMPC) is used to control the full cable-suspended payload system. The NMPC then takes into account the full nonlinear dynamic model of the load-UAV system, along with the constraints of actuators limitation, collision avoidance, and ensuring all cables are taut. However, it is an open question if such an approach works beyond simulation.

A Fly-Crane system is similar to the cable-suspended payload system but using two cables for each quadrotor [7, 20]. This allows the the system to execute a full pose manipulation over the load while attenuating disturbances efficiently. In terms of force allocation and control, each pair of cables is used to define a plane, which is used as input for a local optimizer to compute the angles between these planes with the payload  $x$ - $y$  plane. The optimization uses a gradient-descent iterative algorithm, which is prone to local minima. Unlike our work, no collision avoidance constraints are considered.

One option to solve the nonconvex cable force allocation problem is to convexify the constraints [6]. These constraints

for the force allocation can represent safety distances between the robots or cable tautness guarantees. The method can run online, but the convexification of the constraints is conservative. This might lead to minimizing the space of the force allocation problem.

For redundant systems and specially with multi-task objectives [1, 18], a whole-body force controller is designed to optimize control force allocation over the actuators of such systems. Typically, the objective is to achieve hybrid position/force control, considering multi-task optimization under hard-constraints. Thus, the authors proposed a quadratic programming optimization formulation that can handle different types of constraints such as physical interactions, actuators limits, and additional tasks.

In this paper, we address the shortcomings by augmenting the existing controllers [8, 10] with quadratic programming optimization to allocate the cable forces while taking into account load distribution and inter-robot collisions, while retaining the existing stability results. Moreover, unlike the previous work, we demonstrate our approach in physical test flights.

### III. BACKGROUND

#### A. Single Quadrotor Dynamics

The dynamics of a single multirotor is modeled as a 6 degrees-of-freedom floating rigid body with mass  $m$  and diagonal moment of inertia  $\mathbf{J}$ . The quadrotor's state comprises of the global position  $\mathbf{p} \in \mathbb{R}^3$ , global velocity  $\mathbf{v} \in \mathbb{R}^3$ , attitude rotation matrix  $\mathbf{R} \in SO(3)$  and body angular velocity  $\boldsymbol{\omega} \in \mathbb{R}^3$ . The dynamics can be expressed using Newton-Euler [17] equations of motion as follows

$$\dot{\mathbf{p}} = \mathbf{v}, \quad m\mathbf{v} = m\mathbf{g} + \mathbf{R}\mathbf{f}_u, \quad (1a)$$

$$\dot{\mathbf{R}} = \mathbf{R}\hat{\boldsymbol{\omega}}, \quad \mathbf{J}\dot{\boldsymbol{\omega}} = \mathbf{J}\boldsymbol{\omega} \times \boldsymbol{\omega} + \boldsymbol{\tau}_u, \quad (1b)$$

where  $\hat{\cdot}$  denotes a skew-symmetric mapping  $\mathbb{R}^3 \rightarrow \mathfrak{so}(3)$ ;  $\mathbf{g} = (0, 0, -g)^T$  is the gravity vector;  $\mathbf{f}_u = (0, 0, f)^T$  and  $\boldsymbol{\tau}_u = (\tau_x, \tau_y, \tau_z)^T$  are the total thrust and body torques from the rotors, respectively. The total wrench vector applied on the center-of-mass (CoM) of the quadrotor's body is defined as  $\boldsymbol{\eta} = (f, \tau_x, \tau_y, \tau_z)^T$ . The total wrench vector  $\boldsymbol{\eta}$  is linearly related to the squared motor rotational rate (i.e., propeller speed) for  $k$  motors, such that  $\boldsymbol{\omega}_m = (w_1^2, \dots, w_k^2)^T$ , such that  $\boldsymbol{\eta} = \mathbf{B}_0\boldsymbol{\omega}_m$ , where  $\mathbf{B}_0$  is the actuation matrix [17].

#### B. Full System Dynamics

Consider a team of  $n$  quadrotors that are connected to a payload through massless cables (see Fig. 1). In the following, we summarize results presented in [8, 10] using our own notation for clarity. Throughout this work, the variables related to the payload are denoted by the subscript 0, and the variables for the  $i$ -th quadrotor are denoted by the subscript  $i \in \{1, \dots, n\}$ . The payload is described as a rigid body with mass  $m_0$  and moment of inertia matrix  $\mathbf{J}_0$ . The cables are assumed to be always taut (i.e., modeled as rigid rods) each with length  $l_i$ . The states of the full system can be described as the global

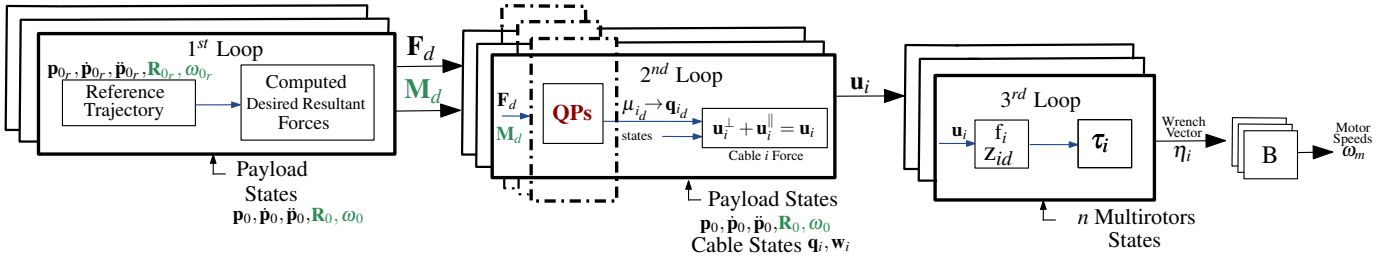


Fig. 2. Controller architecture of the state-of-the-art geometric controller for payload transport. We contribute an optimization-based cable force allocation (shown in red). Green states are only needed when transporting a rigid body rather than a point mass.

position  $\mathbf{p}_0 \in \mathbb{R}^3$  and the velocity  $\dot{\mathbf{p}}_0 \in \mathbb{R}^3$  of the payload; the attitude rotation matrix  $\mathbf{R}_0 \in SO(3)$  and the body angular velocity  $\boldsymbol{\omega}_0 \in \mathbb{R}^3$  of the payload; the unit directional vector  $\mathbf{q}_i \in \mathbb{R}^3$  and the angular velocity  $\boldsymbol{\omega}_i \in \mathbb{R}^3$  of each  $i$ -th cable, where  $\mathbf{q}_i$  points from quadrotor  $i$  towards the payload. Hence, the state space has dimension  $13 + 6n$ .

Consider the full cable-suspended payload system and let us define the attachment point vectors between each cable and the payload as  ${}^0\mathbf{p}_{a_i}$  expressed in the payload frame of reference. Given the states of the full system, the position of each quadrotor expressed in the fixed global frame is  $\mathbf{p}_i = \mathbf{p}_0 + \mathbf{R}_0 {}^0\mathbf{p}_{a_i} - l_i \mathbf{q}_i$ . Thus, the kinematics of the full system is described as

$$\begin{aligned} \dot{\mathbf{q}}_i &= \boldsymbol{\omega}_i \times \mathbf{q}_i, & \dot{\mathbf{p}}_i &= \dot{\mathbf{p}}_0 + \dot{\mathbf{R}}_0 {}^0\mathbf{p}_{a_i} - l_i \dot{\mathbf{q}}_i \\ \dot{\mathbf{R}}_0 &= \mathbf{R}_0 \hat{\boldsymbol{\omega}}_0, \end{aligned} \quad (2)$$

and the nonlinear dynamics of the full system can be expressed using Euler-Lagrange equations.

### C. Control Design

1) *Single Quadrotor without Payload*: Consider a single quadrotor control problem: the goal is to compute propeller speeds such that a given a tuple reference trajectory  $\langle \mathbf{p}_r, \dot{\mathbf{p}}_r, \ddot{\mathbf{p}}_r, \psi_r \rangle$  for the quadrotor CoM is tracked. Here,  $\mathbf{p}_r$  and  $\psi_r$  are the position and the heading of the quadrotor, respectively. The controller in [9] is developed for the single quadrotor case and consists of 2-loop cascaded design, where the outer loop computes the desired force control vector, which then computes  $f$  and the desired third body  $z$ -axis  $z_d$ . Thus, using differential flatness along with the the reference heading  $\psi_r$ , the desired rotational states are computed and  $\boldsymbol{\tau}_u$  is used to track those desired states [17, 9].

2) *Control Design for Payload Dynamics*: In order to achieve a controller for multi-UAVs transporting a shared payload, the single control design is not applicable for this case, as it does not consider the dynamics of the cable-suspended payload system.

The geometric controller by Lee [8] solves the multi-UAVs shared payload transportation problem, where the control problem is defined as follows. The input is a tuple reference trajectory  $\langle \mathbf{p}_0, \dot{\mathbf{p}}_0, \ddot{\mathbf{p}}_0, \mathbf{R}_0, \boldsymbol{\omega}_0 \rangle$ , where  $\mathbf{p}_0, \mathbf{R}_0, \boldsymbol{\omega}_0$  are the position, rotation matrix and angular velocity of the payload, respectively. The output is a collaborative/centralized

controller that computes the motor signals for each robot to track this reference trajectory.

*Desired Payload Forces and Moments*: This controller consists of a 3-loop cascaded design as shown in Fig. 2. The first step in the first loop computes the desired resultant control forces,  $\mathbf{F}_d$ , and torques,  $\mathbf{M}_d$ , of the payload to track the payload reference trajectory. Then, the first loop outputs the desired cable unit directional vectors  $\mathbf{q}_{i_d}$  in order to achieve  $\mathbf{F}_d$  and  $\mathbf{M}_d$ . Let  $\boldsymbol{\mu}_{i_d}$  be the desired  $i$ -th cable force and  $\mathbf{P} \in \mathbb{R}^{6 \times 3n}$  be a matrix that maps the forces and torques of the payload CoM to desired cable forces  $\boldsymbol{\mu}_{i_d}$  on the attachment points  $\mathbf{p}_{a_i}$ . Thus,  $\mathbf{P}$  is a constant matrix structured from  $\mathbf{p}_{a_i}$ , refer to Lee [8] for details.

The cable force allocation relation between  $\boldsymbol{\mu}_{i_d}$  and  $\mathbf{F}_d, \mathbf{M}_d$  is defined as

$$\mathbf{P} ((\mathbf{R}_0^T \boldsymbol{\mu}_{1_d})^T \dots (\mathbf{R}_0^T \boldsymbol{\mu}_{n_d})^T) = ((\mathbf{R}_0^T \mathbf{F}_d)^T \quad \mathbf{M}_d^T)^T. \quad (3)$$

3) *Cable Force Allocation*: For any  $\mathbf{F}_d, \mathbf{M}_d$  and  $n \geq 3$ , there exist desired cable forces  $\boldsymbol{\mu}_{i_d}$ . These desired cable forces can be computed using the Moore-Penrose inverse of  $\mathbf{P}$  to achieve a least-square solution:

$$\boldsymbol{\mu}_{i_d} = \text{diag}(\mathbf{R}_0, \dots, \mathbf{R}_0) \mathbf{P}^T (\mathbf{P} \mathbf{P}^T)^{-1} \begin{pmatrix} \mathbf{R}_0^T \mathbf{F}_d \\ \mathbf{M}_d \end{pmatrix}. \quad (4)$$

*Point Mass Model*: If we consider the special case of the payload being a point mass, then the controller architecture retains the same structure, see Fig. 2. However, since we only include the translational dynamics, the force allocation relation reduces to

$$\mathbf{P} (\boldsymbol{\mu}_{1_d}^T \quad \dots \quad \boldsymbol{\mu}_{n_d}^T)^T = \mathbf{F}_d. \quad (5)$$

4) *Control Inputs of the UAVs*: Let the control force applied by each  $i$ -th quadrotor on its cable be  $\mathbf{u}_i = \mathbf{R}_i \mathbf{f}_{u_i}$ . Denote that  $\mathbf{u}_i^\parallel \in \mathbb{R}^3$  and  $\mathbf{u}_i^\perp \in \mathbb{R}^3$  are the orthogonal projection of  $\mathbf{u}_i$  along  $\mathbf{q}_i$  and to the plane normal to  $\mathbf{q}_i$ , respectively, i.e.,  $\mathbf{u}_i = \mathbf{u}_i^\parallel + \mathbf{u}_i^\perp$ . We compute  $\mathbf{q}_{i_d}$  using the desired cable forces  $\boldsymbol{\mu}_{i_d}$  by applying the definition

$$\mathbf{q}_{i_d} = \frac{\boldsymbol{\mu}_{i_d}}{\|\boldsymbol{\mu}_{i_d}\|}. \quad (6)$$

The second loop computes the control force  $\mathbf{u}_i$  applied by each quadrotor on the payload. In particular,  $\mathbf{u}_i^\parallel$  is first computed by projecting  $\boldsymbol{\mu}_{i_d}$  on the current cable force vector  $\boldsymbol{\mu}_i$ , in addition to non-linear terms that linearize the translational dynamics of

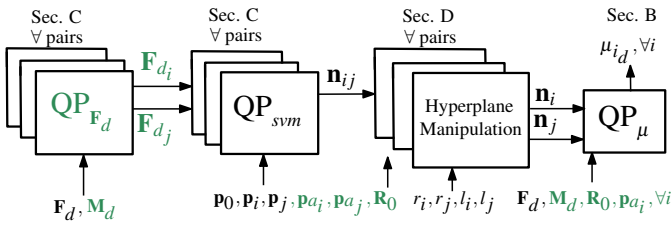


Fig. 3. Our cable force allocation method uses three QPs. The final QP,  $QP_\mu$ , computes the desired cable forces  $\mu_{i_d}$  by constraining them to fulfill the allocation constraints Eq. (5) (point mass) or Eq. (3) (rigid body) and limiting them to be inside a polyhedra defined by a set of hyperspaces. These hyperspaces are constructed by two other QPs that are solved for each robot pair,  $QP_{svm}$  and  $QP_{F_d}$ . Green parts are not needed for the point mass case.

the payload. In other words, when  $\mu_i \rightarrow \mu_{i_d}$ , then  $F_d, M_d$  are tracked. In order to track the desired cable forces  $\mu_{i_d}$ , the vector  $u_i^\perp$  is used to track the desired unit directional vector, i.e.,  $q_i \rightarrow q_{i_d}$ , of the cables. When  $q_i = q_{i_d}$  then the resultant force and moment acting on the payload become identical to their desired values.

After computing  $u_i$ , the final third loop computes the thrust magnitude  $f$  (i.e.,  $f_u$ ) and the desired third body vector  $z_d$ . Thus, using differential flatness, we can define the desired rotation matrix and its derivatives and compute the attitude control input  $\tau_u$  to track the desired attitude values. This third loop is identical with the second loop of the single quadrotor geometric controller.

#### D. Quadratic Programs and Hyperplanes

A quadratic program (QP) is an optimization problem with a quadratic objective and affine equality and inequality constraints. The QP is formulated as

$$\begin{aligned} \min_x \quad & \frac{1}{2} x^T P x + q^T x \\ \text{s.t.} \quad & l \leq A x \leq u \end{aligned} \quad (7)$$

where  $x \in \mathbb{R}^n$  is the decision variable vector. The objective function is defined by a positive semi-definite matrix  $P \in \mathbb{R}^{n \times n}$  and  $q \in \mathbb{R}^n$ . The linear constraints are defined by matrix  $A \in \mathbb{R}^{m \times n}$  and vectors  $l$  and  $u$  such that  $l_i \in \mathbb{R} \cup \{-\infty\}$  and  $u_i \in \mathbb{R} \cup \{+\infty\}$  for all  $i \in (1, \dots, m)$ . QPs are convex and thus find a global minima.

A hyperplane  $\mathcal{H}$  in  $\mathbb{R}^d$  can be formulated by a normal vector  $\mathbf{n}$  and an offset  $a$  as  $\mathcal{H} = \{x \in \mathbb{R}^d \mid \mathbf{n}^T x - a = 0\}$ . A half-space  $\tilde{\mathcal{H}}$  in  $\mathbb{R}^d$  is a subset of  $\mathbb{R}^d$  that is bounded by a hyperplane such that  $\tilde{\mathcal{H}} = \{x \in \mathbb{R}^d \mid \mathbf{n}^T x - a \leq 0\}$ . The intersection of multiple hyperspaces creates a polyhedra. Hyperplanes can be used as a linear constraints for a QP formulation.

### IV. APPROACH

#### A. Overview

We augment the existing geometric controller described in Section III-C with a custom force allocation method (replacing the standard approach presented in Section III-C3) to achieve

trajectories for the quadrotors that avoid inter-robot collisions. As such, we provide a drop-in replacement for Eq. (4), that is we use the desired force on the payload,  $F_d$ , and the desired moments for the payload,  $M_d$ , as input and compute the desired cable forces,  $\mu_{i_d}$ , while taking inter-robot collision avoidance into account. The nonlinear optimization problem formulation can be defined as,

$$\begin{aligned} \min_{\mu_{i_d}} \quad & \frac{1}{2} \|\mu_{i_d}\|^2 \\ \text{s.t.} \quad & \begin{cases} (3) \text{ or } (5) \\ \|\mathbf{p}_i(\mu_{i_d}, \cdot) - \mathbf{p}_j(\mu_{i_d}, \cdot)\| \geq r_i + r_j, \quad \forall i \neq j, \end{cases} \end{aligned} \quad (8)$$

where  $\mathbf{p}_i(\mu_{i_d}, \cdot)$  and  $\mathbf{p}_j(\mu_{i_d}, \cdot)$  are the positions of each pair of quadrotors and  $r_i, r_j$  are safety radii. Consider the tracking of the desired cable directions  $q_{i_d}$  is fast enough such that  $q_i = q_{i_d}$ . Then  $\mathbf{p}_i$  and  $\mathbf{p}_j$  can be described as a function of  $\mu_{i_d}$  (see Eq. (6)) and other nonlinear terms expressed with  $(\cdot)$ . The first constraint enforces the force allocation constraints for the point mass or rigid body payload case, respectively. The second constraint ensures that the safety distance between each pair of  $i$  and  $j$  quadrotors is at least  $r_i + r_j$ .

Without the second constraint, the optimal solution in the least square sense of the desired cable force allocation is provided by Eq. (4). Instead of using a nonlinear optimization that solves for  $\mu_{i_d}$  subject to the second nonconvex constraint, we use a cascaded design of three quadratic programs (QPs) to link these variables implicitly, see Fig. 3. The first three blocks in Fig. 3 run on each quadrotor for all robot pairs. Thus, for  $n$  quadrotors, these blocks are executed  $n(n-1)/2$  times.

Our key insight is to construct hyperplanes that separate each pair of quadrotors. These hyperplanes should also take the desired motion of the payload (i.e.,  $F_d, M_d$ ) into account. We use the first block,  $QP_{F_d}$ , for each pair to provide heuristics of desired cable forces ( $F_{d_i}$  and  $F_{d_j}$ ) as if each pair is achieving the desired payload motion by itself. The next block,  $QP_{svm}$ , constructs a hyperplane to separate the two corresponding cables with a preference for solutions such that the desired  $F_{d_i}$  and  $F_{d_j}$  can be achieved. Since the resulting hyperplane between each pair might have a very small safety margin, we use geometric hyperplane manipulation (third block) to construct two new hyperplanes, one for each quadrotor of the pair, that possess the desired safety distance and constrains the desired cable forces  $\mu_{i_d}$ .

Finally the last block  $QP_\mu$  runs once on each quadrotor to allocate the desired cable forces  $\mu_{i_d}$  for the full cable system, and each quadrotor extracts its own solution from  $QP_\mu$ .

#### B. QP For Desired Cable Forces ( $QP_\mu$ )

The minimum-norm solution of Eq. (3) or Eq. (5) will provide a solution for  $\mu_{i_d}$ . We add additional (hard) constraints to the optimization problem. The resulting optimization problem is a QP due to the linear constraints and can be solved

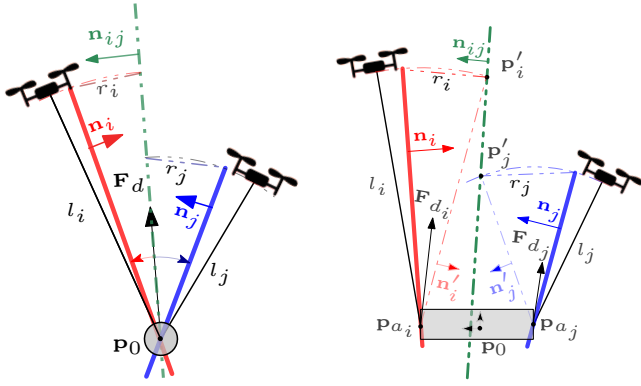


Fig. 4. 2D projection of the hyperplane manipulation, where  $\text{QP}_{svm}$  computed  $\mathbf{n}_{ij}$ . Left: Point mass case, where  $\mathbf{n}_{ij}$  is rotated around  $\mathbf{p}_0$  such that the distance to  $\mathbf{n}_{ij}$  is  $r_i$  or  $r_j$ . Right: Rigid body case, where new intermediate hyperplanes  $\mathbf{n}'_i$  and  $\mathbf{n}'_j$  are constructed followed by the same rotation as in the point mass case.

efficiently:

$$\begin{aligned} \min_{\boldsymbol{\mu}_{id}} \quad & \frac{1}{2} \|\boldsymbol{\mu}_{id}\|^2 \\ \text{s.t.} \quad & \begin{cases} (3) \text{ or } (5) \\ \begin{pmatrix} \mathbf{n}_1^T & \dots & 0 \\ 0 & \ddots & 0 \\ 0 & \dots & \mathbf{n}_m^T \end{pmatrix} \begin{pmatrix} \boldsymbol{\mu}_{1d} \\ \vdots \\ \boldsymbol{\mu}_{md} \end{pmatrix} - \begin{pmatrix} a_1 \\ \vdots \\ a_m \end{pmatrix} \leq \mathbf{0}_{m \times 1} \end{cases} \end{aligned} \quad (9)$$

where  $\mathbf{n}_i \in \mathbb{R}^{3 \times 1}$  and  $a_i \in \mathbb{R}$  for  $i \in 1, \dots, m$  define a the constraining half-spaces and  $m$  is the number of hyperplanes with  $m \geq n$ .

### C. QPs for Hyperplanes ( $\text{QP}_{svm}$ ) and Force Pairs ( $\text{QP}_{\mathbf{F}_d}$ )

In the  $\text{QP}_{\boldsymbol{\mu}}$  formulation, our inequality constraints are formulated using hyperplanes. We compute these hyperplanes by solving another QP followed by geometric manipulation to construct a constraint for the cable forces. Consider each pair of robots  $i$  and  $j$ . Their positions are as  ${}^0\mathbf{p}_i$  and  ${}^0\mathbf{p}_j$  in the payload frame of reference. For better readability, we omit the superscripts of the robot position vectors in the payload frame, and use them as  $\mathbf{p}_i$  and  $\mathbf{p}_j$ .

1) *Point Mass Model*: For each pair of robots we generate two hyperplanes  $\mathbf{n}_i$  and  $\mathbf{n}_j$ , see Fig. 4 on the left. In order to generate these hyperplanes, we first need to compute for each pair the hyperplane  $\mathbf{n}_{ij}$  that separates both robots while being as close as possible to  $\mathbf{F}_d$ . Thus,  $\mathbf{n}_{ij}$  is responsible to maximize the safety margin between the positions of the robots while regularizing for  $\mathbf{F}_d$ . This regularization term generates  $\boldsymbol{\mu}_{id}$  such that the desired force can be tracked well in the sense of generating the hyperplanes to provide spaces of motion for the cables in the same direction of the desired  $\mathbf{F}_d$ . Afterwards,  $\mathbf{n}_{ij}$  is used to compute both  $\mathbf{n}_i$  and  $\mathbf{n}_j$  to be used in  $\text{QP}_{\boldsymbol{\mu}}$ .

We adopt a variation of multi-objective hard-margin support vector machines (SVM) with additional regularization for  $\mathbf{F}_d$

as  $\text{QP}_{svm}$ :

$$\begin{aligned} \min_{\mathbf{n}_{ij}} \quad & \|\mathbf{n}_{ij}\|^2 + \lambda_s (\mathbf{n}_{ij}^T \mathbf{F}_d)^2 \\ \text{s.t.} \quad & \begin{cases} \mathbf{n}_{ij}^T \mathbf{p}_i \leq -1 \\ \mathbf{n}_{ij}^T \mathbf{p}_j \geq 1 \end{cases} \end{aligned} \quad (10)$$

Here,  $\lambda_s$  is a weighting factor for the soft constraint that acts as a trade-off between the safety margin and the hyperplane of  $\mathbf{n}_{ij}$  being as close to  $\mathbf{F}_d$ . In fact, a high  $\lambda_s$  might result in a safety margins that are close to zero. Our formulation implicitly constrains the plane to pass through the payload by not including an offset  $a$  in the  $\text{QP}_{svm}$ . If such an offset is included, then the hyperplanes might be shifted and consequently, this might render  $\text{QP}_{\boldsymbol{\mu}}$  infeasible.

2) *Rigid Body Model*: For the rigid body case (Fig. 4 on the right) we use the attachment points between each cable and the payload as  $\mathbf{p}_a$ . Recall that the positions of the robots and the attachment points of each cable are  $\mathbf{p}_i, \mathbf{p}_j, \mathbf{p}_{a_i}, \mathbf{p}_{a_j}$  in the payload frame of reference, respectively. Similar to the point mass model, our objective is to find the hyperplanes  $\mathbf{n}_i$  and  $\mathbf{n}_j$  that set the desired safety distances between the robots. We start by solving a  $\text{QP}_{svm}$  for  $\mathbf{n}_{ij}$  that separates each pair of cables. However, in the rigid payload case, other than requiring the hyperplane to be as close to  $\mathbf{F}_d$ , we also need to take into account the desired computed moments  $\mathbf{M}_d$ . Thus we propose that for each pair of robots we first solve a  $\text{QP}_{\mathbf{F}_d}$  that solves for  $\mathbf{F}_{d_i}$  and  $\mathbf{F}_{d_j}$  to be applied on the attachment points  $\mathbf{p}_{a_i}$  and  $\mathbf{p}_{a_j}$ . The sum of these forces must achieve  $\mathbf{F}_d$  while producing moments to be close to  $\mathbf{M}_d$ . Let us define  $\hat{\mathbf{p}}_{a_i}$  and  $\hat{\mathbf{p}}_{a_j}$  as the skew-symmetric mapping of  $\mathbf{p}_{a_i}$  and  $\mathbf{p}_{a_j}$ , then  $\mathbf{F}_{d_i}$  and  $\mathbf{F}_{d_j}$  can be solved as

$$\begin{aligned} \min_{\mathbf{F}_{d_i}, \mathbf{F}_{d_j}} \quad & \|\mathbf{F}_{d_i}\|^2 + \|\mathbf{F}_{d_j}\|^2 + \\ & \|\mathbf{M}_d - (\hat{\mathbf{p}}_{a_i} \mathbf{R}_0^T \mathbf{F}_{d_i} + \hat{\mathbf{p}}_{a_j} \mathbf{R}_0^T \mathbf{F}_{d_j})\|^2 \\ \text{s.t.} \quad & \mathbf{F}_{d_i} + \mathbf{F}_{d_j} = \mathbf{F}_d. \end{aligned} \quad (11)$$

Since we only solve for two force vectors  $\mathbf{F}_{d_i}$  and  $\mathbf{F}_{d_j}$ , we may not find an exact solution to achieve both  $\mathbf{F}_d$  and  $\mathbf{M}_d$ . Thus, we prioritize to solve for  $\mathbf{F}_d$  by considering it as a hard constraint and add a soft constraint to have a solution as close as possible to  $\mathbf{M}_d$ .

After solving for  $\mathbf{F}_{d_i}$  and  $\mathbf{F}_{d_j}$ , we use a hybrid soft-hard margin SVM. In particular, we want to solve for the normal of the hyperplane  $\mathbf{n}_{ij}$  and an offset  $a$ . Note that there is no particular desired intersection point between the  $\mathbf{n}_{ij}$  hyperplane and the rigid payload, thus  $a$  is a decision variable. Accordingly, we propose the following  $\text{QP}_{svm}$ :

$$\begin{aligned} \min_{\mathbf{n}_{ij}, a, s_1, s_2} \quad & \|\mathbf{n}_{ij}\|^2 + \lambda_s (s_1 + s_2) \\ \text{s.t.} \quad & \begin{cases} \mathbf{n}_{ij}^T \mathbf{p}_i - a \leq -1, & \mathbf{n}_{ij}^T \mathbf{p}_j - a \geq 1 \\ \mathbf{n}_{ij}^T \mathbf{p}_{a_i} - a \leq -1, & \mathbf{n}_{ij}^T \mathbf{p}_{a_j} - a \geq 1 \\ \mathbf{n}_{ij}^T (\mathbf{p}_{a_i} + \mathbf{F}_{d_i} - a) \leq -1 + s_1 \\ \mathbf{n}_{ij}^T (\mathbf{p}_{a_j} + \mathbf{F}_{d_j} - a) \geq 1 - s_2 \\ s_1 \geq 0, & s_2 \geq 0 \end{cases} \end{aligned} \quad (12)$$

Here, the first four constraints separate the cables like in a hard-margin SVM. The next six constraints assure that the hyperplane  $\mathbf{n}_{ij}$  minimizes the projection of both  $\mathbf{F}_{d_i}$  and  $\mathbf{F}_{d_j}$  after being shifted on the attachment points  $\mathbf{p}_{a_i}, \mathbf{p}_{a_j}$  respectively. We use two slack variables  $s_1$  and  $s_2$  as another term in the cost function. These slack variables are minimized to relax the hard constraints imposed on the projection of  $\mathbf{F}_{d_i}$  and  $\mathbf{F}_{d_j}$  on the hyperplane of  $\mathbf{n}_{ij}$ . This part is similar to a soft-margin SVM.

Similar to the point mass case,  $\lambda_s$  also acts as a trade-off between the safety margin and being close to both forces. We include the offset  $a$  of the plane as a decision variable, thus, the hyperplane does not have to pass through the CoM  $\mathbf{p}_0$ .

#### D. Hyperplane Manipulation

After computing the separating hyperplane  $\mathbf{n}_{ij}$ , we need to compute  $\mathbf{n}_i$  and  $\mathbf{n}_j$  normals of the hyperplanes as constraints for the QP in Eq. (9), see Fig. 4. For both cases, it is worth noting that the solution of the  $\mathbf{n}_{ij}$  vector is always directed towards  $\mathbf{p}_i$ .

1) *Point Mass Model*: Given the radius of each robot  $r_i$  and  $r_j$  and the length of each cable  $l_i$  and  $l_j$ , we first compute the angles  $\alpha_i$  and  $\alpha_j$  by using the properties of the resulting isosceles triangle as

$$\alpha_i = 2 \arcsin\left(\frac{r_i}{2l_i}\right), \quad \alpha_j = 2 \arcsin\left(\frac{r_j}{2l_j}\right). \quad (13)$$

Let us define  $\mathbf{e}_3 = (0, 0, 1)^T$  and define quaternions  $\mathbf{q}_i$  and  $\mathbf{q}_j$  by converting the axis-angle representation to a quaternion using the axis  $\mathbf{n}_{ij} \times \mathbf{e}_3$  with the angles  $\alpha_i$  and  $-\alpha_j$ . Finally, we compute the normals  $\mathbf{n}_i$  and  $\mathbf{n}_j$  by tilting  $\mathbf{n}_{ij}$  with the computed  $\mathbf{q}_i$  and  $\mathbf{q}_j$ . Let us define the  $\odot$  as the quaternion rotation operator, then  $\mathbf{n}_i$  and  $\mathbf{n}_j$  are

$$\mathbf{n}_i = \mathbf{q}_i \odot \mathbf{n}_{ij}, \quad \mathbf{n}_j = -\mathbf{q}_j \odot \mathbf{n}_{ij}. \quad (14)$$

Note that it is required by the QP which solves for  $\mu_{i_d}$  that both normals must be pointing inwards (i.e., towards each other), which explains the negative sign add in the  $\mathbf{n}_j$  normal computation in Eq. (14).

2) *Rigid Body Model*: We use the same method for tilting but we add other steps. Let us define two points  $\mathbf{p}'_i$  and  $\mathbf{p}'_j$  as shown in Fig. 4 on the right. We first compute the intersection between the sphere that describes the motion of each cable and the hyperplane  $\mathbf{n}_{ij}$ . The result is a circle on  $\mathbf{n}_{ij}$ . We use the points of the circle with the highest  $z$ -coordinate as  $\mathbf{p}'_i$  and  $\mathbf{p}'_j$ . Afterwards, two new hyperplanes are computed as  $\mathbf{n}'_i$  and  $\mathbf{n}'_j$  by using vector  $\mathbf{n}_{ij} \times \mathbf{e}_3$  and two points for each plane, which are the intersection points  $\mathbf{p}'_i$  and  $\mathbf{p}'_j$  and the attachment points  $\mathbf{p}_{a_i}, \mathbf{p}_{a_j}$ , respectively. Finally, we apply the same steps from the point mass case to tilt  $\mathbf{n}'_i$  and  $\mathbf{n}'_j$  based on the radii  $r_i$  and  $r_j$  of each robot model to generate  $\mathbf{n}_i$  and  $\mathbf{n}_j$  using Eq. (13) and Eq. (14).

#### E. Desired Cable Forces

One of the main advantages of the  $\text{QP}_\mu$  formulation and in particular the choice of representing the inequality constraints

are the extensions that provide new use-cases. Here, we provide one such example to provide desired cable forces. There are two motivations behind supporting this feature. The first motivation is to steer the optimization problem to have a more continuous solution for the decision variables that avoids any sudden jumps between two consecutive solutions. The second motivation is to allow the user to specify a desired formation configuration, for example to pass through a narrow passage.

Let us define  $\mu_{i_0}$  as preferable desired cable forces, as either the solution from the previous optimization or the user-specified desired values. In the latter case, we can rescale  $\mu_{i_0}$  such that  $\sum_i \mu_{i_0} = \mathbf{F}_d$ . The cost function in  $\text{QP}_\mu$  (Eq. (9)) can be modified to minimize the difference between the desired cable forces and the preferred ones as

$$c = \frac{1}{2} \|\mu_{i_d}\|^2 + \lambda \|\mu_{i_0}^T - \mu_{i_d}\|^2, \quad (15)$$

where  $\lambda$  is a weighting factor for the second term of the cost function.

## V. EXPERIMENTS

To validate the functionality of our proposed methodology, we present our development workflow for sim-to-real transfer as well as experimental results on a physical team of up to three quadrotors transporting different payloads.

#### A. Target Platform

We use quadrotors of type Bitcraze Crazyflie 2.1 (CF). These are small (9 cm rotor-to-rotor) and lightweight (34 g) products that are commercially available. The physical parameters are identified in prior work [4]. We use the existing extended Kalman filter for state estimation and implement our control algorithm in *C* to run directly on-board the STM32-based flight controller (168 MHz, 192 kB RAM).

#### B. Sim-to-Real Development Process

We found that an iterative development method reduces challenges regarding the sim-to-real gap. We developed and tuned our approach through four stages.

In the first stage, we implement our experiments in simulation using only *Python*. We start with the dynamic model of a single quadrotor and a state-of-the-art single UAV controller [9]. Then, we extend the simulation to the multi-UAVs payload transportation problem using the dynamics from Section III-B. In all cases we found that a simple Euler Integration method and a small timestep provide reasonable results. All physical parameters used in the simulation for the quadrotor are based on an existing system identification [4]. Finally, we implement the baseline Eq. (4) and our approach using QPs. For our controller, we write the QP program using an open source Python-embedded modeling language for convex optimization problems, CVXPY [3].

In the second stage, we port our baseline controller from *Python* to *C* and add it to the quadrotor's firmware. Then, we generate Python bindings for the relevant firmware code using SWIG. We verify the semantic equivalence between the

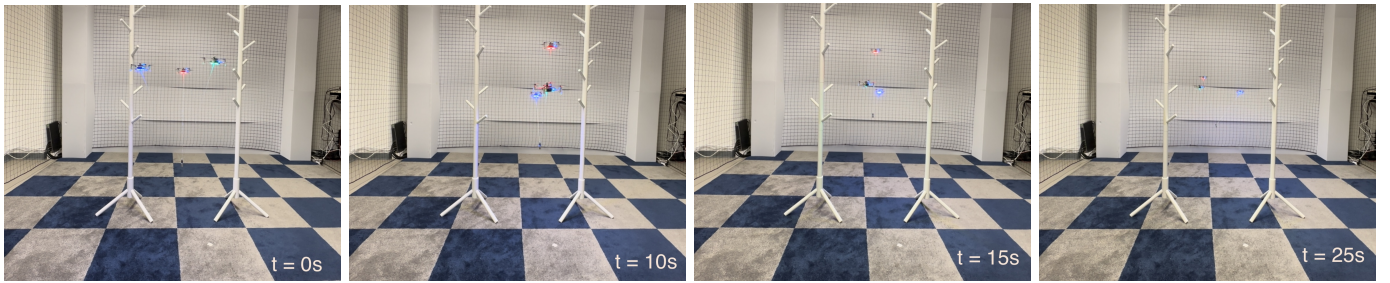


Fig. 5. Four frames of three quadrotors carrying a point mass payload in a teleoperation use-case. There are two obstacles forming a narrow passage. The operator controls the payload position as well as the desired formation. Here, a line configuration as shown in  $t = 10s$  and  $t = 15s$  is used. After passing the obstacles, the operator disables the manual formation control and our approach computes to a more energy-efficient triangle formation ( $t = 25s$ ).

two implementations by using those Python bindings in our simulator in a Software-in-The-Loop (SITL) fashion.

In the third stage, we port our own controller, which requires to solve multiple QPs (Eq. (9)) on-board the STM32 microcontroller. The primary challenge is to migrate our QP formulations from CVXPY to C. The most obvious choice, CVXPYgen<sup>1</sup>, was not able to generate code for all of our QPs. Instead, we re-write our QPs using the OSQP (Operator Splitting Quadratic Program) solver [23], which is one of the underlying solvers that CVXPY can task with solving QPs. However, OSQP requires the users to specify matrices and vectors to construct the problem, which is more error-prone than CVXPY’s mathematical modeling language. We use the data that CVXPY produces for example problems as inspiration for constructing the OSQP problems. One major advantage of OSQP is that it can generate tailored C code that compiles into a fast and reliable solver for the given family of QP problems in which the problem data, but not its dimensions, change between problem instances. Moreover, the generated code is optimized for embedded systems, i.e., only uses static allocations. With minor modifications to support multiple different QPs in one binary, this generated code can be easily integrated to the existing STM32 firmware. As before, we verify the semantic equivalence between the pure Python version and our C implementation using test cases.

In the fourth stage, we optimize the code to be able to run in realtime on the physical hardware. To this end, we avoid some implicit double-precision variable promotions and limit ourselves to single-precision floating point operations. In addition, we solve the generated QPs asynchronously, separately from the rest of the controller that runs at 250 Hz by employing FreeRTOS tasks and queues for exchange of input/output data. Finally, we store the primal and dual results for each QP and warm start the optimization with these values.

### C. Physical Flights

We verify our approach in physical flight tests with up to three Crazyflies. Each multirotor has its own controller running on-board, solving the QPs and using the computed desired cable forces for itself to generate its own control input for the motors. Such a distributed execution requires that all

robots compute identical values. Since our QPs have a global minimum that the solver reaches, we just need to ensure that all multirotors use the same input data. On the host side, we use CrazySwarm2<sup>2</sup>, which is based on CrazySwarm [21] but uses ROS2 [14] to control and send commands for multiple Crazyflies. CrazySwarm2 heavily relies on broadcast communication for state estimation and control commands, which ensures that all robots receive the data at the same time. In particular, we equip each quadrotor with a single reflective marker for position tracking at 100 Hz using an OptiTrack motion capture system. For the payload we use a single marker for the pointmass or let the motion capture track the rigid body payload. The resulting multirotor positions and payload pose are send using broadcasts to all robots. For commands such as takeoff, land, or trajectory execution we also rely on broadcasts to ensure consistent desired states between multirotors.

The states of each quadrotor are estimated on-board using an extended Kalman filter and the first derivatives of the payload state using numeric differentiation in combination with a complimentary filter. For the payload, we use a calibration weight as point mass, cardboard and 3D-printed objects as rigid bodies, and dental floss as cables. Cables and payload/multirotor are connected to each other with magnets for easy exchange and repairability.

1) *Experimental Results:* We conduct several real flight experiments, as summarized in Table I. We choose the experiments such that the baseline using Eq. (4) to compute the desired cable forces would result in catastrophic crashes, as it is unaware of the physical dimensions of the robots and the payload. For each case, we report the runtime of our optimization (as executed on-board the microcontroller), the position error of the payload, and the orientation error of the payload.

We consider two different types of reference motions: a pre-planned polynomial figure-8 trajectory (reaching 0.5 m/s for the point mass and 0.4 m/s for the rigid body cases), and teleoperation with position and velocity commands for the payload. For the the teleoperation experiment, we put obstacles as shown in Fig. 5 such that the robots need to switch to a line configuration (see Section IV-E) to avoid collisions. The operator was able to switch to a predefined configuration by

<sup>1</sup><https://github.com/cvxgrp/cvxpygen>

<sup>2</sup><https://imrclab.github.io/crazyswarm2>

TABLE I  
FLIGHT TEST RESULTS. SHOWN ARE MEAN VALUES OVER TIME FOR A SINGLE FLIGHT EACH WITH STANDARD DEVIATION (SMALL GRAY).

	2 UAVs, point mass	3 UAVs, point mass	2 UAVs, rod	3 UAVs, triangle	3 UAVs, point mass
Payload	point mass	point mass	rod	triangle	point mass
Trajectory	figure 8 (13 s)	figure 8 (13 s)	figure 8 (15 s)	figure 8 (15 s)	teleoperation
Mass [g]	10	10	8	10	10
Dimension [cm]	-	-	15	8	-
Cables [cm]	25, 50	25, 50, 75	50, 50	50, 50, 50	50, 50, 50
QP runtime total [ms]	5.7 <small>1.5</small>	23.1 <small>5.8</small>	13.5 <small>2.1</small>	33.1 <small>4.3</small>	21.8 <small>6.2</small>
QP runtime Fd [ms]	0.0 <small>0.0</small>	0.0 <small>0.0</small>	2.4 <small>0.7</small>	6.9 <small>1.3</small>	0.0 <small>0.0</small>
QP runtime SVM [ms]	2.0 <small>1.2</small>	14.7 <small>4.8</small>	2.7 <small>1.3</small>	8.4 <small>2.9</small>	13.0 <small>4.8</small>
QP runtime $\mu$ [ms]	1.8 <small>0.8</small>	3.9 <small>3.0</small>	3.0 <small>1.2</small>	4.7 <small>2.7</small>	4.4 <small>3.7</small>
Payload x, y, z error [cm]	2.5 <small>1.3</small> , 3.0 <small>2.2</small> , 2.8 <small>1.4</small>	3.6 <small>3.0</small> , 6.3 <small>3.4</small> , 4.0 <small>2.3</small>	4.3 <small>3.4</small> , 3.1 <small>2.4</small> , 4.2 <small>1.7</small>	2.4 <small>1.6</small> , 2.9 <small>1.9</small> , 3.6 <small>1.6</small>	3.0 <small>3.0</small> , 6.8 <small>4.5</small> , 5.9 <small>4.1</small>
Payload r, p, y error [deg]	-	-	6.3 <small>4.5</small> , 6.9 <small>3.9</small> , 20.0 <small>7.3</small>	10.3 <small>4.3</small> , 5.9 <small>3.8</small> , 3.4 <small>1.3</small>	-

pressing a button. For the other experiments, we use two types of rigid payloads and different number of Crazyflies and cable lengths while tracking a figure-8 trajectory.

Overall, we are able to compute desired cable forces at 30 Hz on-board the microcontroller, which is sufficient for robust position- and orientation tracking of the payload. Surprisingly, the overhead of setting up the QPs takes also a significant amount of time (e.g., 13 ms in the 3 UAV triangle case). The obtained position and orientation errors are consistent with prior work using bigger quadrotors [13], for positions in the range of the rotor-to-rotor size of the UAV. The error in the yaw portion of the desired orientation is higher in the 2 UAVs rod case, because of the challenging nature of our yaw setpoints, that require rotating the formation while flying the figure-8 motion.

Videos of all the experiments are provided in the supplemental material.

2) *Challenges*: Executing the baseline and our controller on physical quadrotors was challenging (both [8] and [10] were only shown in simulation).

The baseline controller contained several parts that are numerically unstable for physical flights. The second loop of the controller computes  $\mathbf{u}_i$ , which requires either measuring or estimating the acceleration of the payload. The numeric estimate of this value is very noisy and causes the quadrotors to crash. Instead, we rely on the reference acceleration of the payload. Similarly, the change of the desired cable force direction  $\dot{\mathbf{q}}_{i,d}$  is too noisy in practice and we use  $\mathbf{0}$  instead.

We also found that tuning the gains of the cascaded design is very challenging, even with access to all relevant tracking errors. The gains are very sensitive even to small changes and depend on the number of UAVs and the type of payload. Moreover, recovering from the disturbances that occur during takeoff poses another challenge especially for tuning. We note that switching from the single quadrotor controller to our controller midflight is a possible alternative, but it is not practical for non-uniform cable lengths. Some of these challenges might be easier to overcome on platforms with a higher thrust-to-weight ratio than ours with a low ratio of about 1.4, although our data indicates that motors did only occasionally saturate during takeoff in our experiments. In contrast, the two new gains our method introduces over the

baseline,  $\lambda$  and  $\lambda_s$ , are easy to tune.

## VI. CONCLUSION AND FUTURE WORK

We present an extension to the force allocation of a geometric controller for cable-suspended payload transportation that is aware of neighboring robots to avoid collisions. Unlike previous work that relies on nonlinear optimization, we use a cascaded sequence of small and efficiently solvable quadratic programs. Since we did not change any other parts of the existing controller, the prior stability analysis still holds. We demonstrate that our approach can be executed on compute-constrained multirotors in realtime.

In the future, we are interested in adding additional constraints to support static obstacles or heterogeneous robots. Moreover, an exciting future avenue lies in planning the desired motions and cable forces for time-optimal and collision-free navigation.

## REFERENCES

- [1] Marie Charbonneau, Gabriele Nava, Francesco Nori, and Daniele Pucci. An optimization based control framework for balancing and walking: Implementation on the icub robot. *arXiv preprint arXiv:1707.08359*, 2017.
- [2] Hector Garcia De Marina and Ewoud Smeur. Flexible collaborative transportation by a team of rotorcraft. In *2019 International Conference on Robotics and Automation (ICRA)*, pages 1074–1080. IEEE, 2019.
- [3] Steven Diamond and Stephen Boyd. CVXPY: A Python-embedded modeling language for convex optimization. *Journal of Machine Learning Research*, 17(83):1–5, 2016.
- [4] Julian Förster. System identification of the crazyfly 2.0 nano quadcopter. B.S. thesis, ETH Zurich, 2015.
- [5] Chiara Gabellieri, Marco Tognon, Lucia Pallottino, and Antonio Franchi. A study on force-based collaboration in flying swarms. In *Int. Conf. Swarm Intell.*, pages 3–15, 2018.
- [6] Junyi Geng and Jack W Langelaan. Cooperative transport of a slung load using load-leading control. *Journal of Guidance, Control, and Dynamics*, 43(7):1313–1331, 2020.
- [7] AE Jiménez-Cano, Dario Sanalidro, M Tognon, A Franchi, and J Cortés. Precise cable-suspended

- pick-and-place with an aerial multi-robot system: A proof of concept for novel robotics-based construction techniques. *Journal of Intelligent & Robotic Systems*, 105(3):68, 2022.
- [8] Taeyoung Lee. Geometric control of quadrotor uavs transporting a cable-suspended rigid body. *IEEE Transactions on Control Systems Technology*, 26(1):255–264, 2017.
- [9] Taeyoung Lee, Melvin Leok, and N Harris McClamroch. Geometric tracking control of a quadrotor uav on se (3). In *Proc. IEEE Conf. Decis. Control*, pages 5420–5425, 2010.
- [10] Taeyoung Lee, Koushil Sreenath, and Vijay Kumar. Geometric control of cooperating multiple quadrotor uavs with a suspended payload. In *Proc. IEEE Conf. Decis. Control*, pages 5510–5515, 2013.
- [11] Guanrui Li, Xinyang Liu, and Giuseppe Loianno. RotorTM: A flexible simulator for aerial transportation and manipulation. *arXiv preprint arXiv:2205.05140*, 2022.
- [12] ZuQun Li, Joseph F Horn, and Jack W Langelaan. Coordinated transport of a slung load by a team of autonomous rotorcraft. In *AIAA Guidance, Navigation, and Control Conference*, page 0968, 2014.
- [13] Xinyang Liu, Guanrui Li, and Giuseppe Loianno. Safety-aware human-robot collaborative transportation and manipulation with multiple mavs. *arXiv preprint arXiv:2210.05894*, 2022.
- [14] Steven Macenski, Tully Foote, Brian Gerkey, Chris Lalancette, and William Woodall. Robot operating system 2: Design, architecture, and uses in the wild. *Science Robotics*, 7(66), 2022.
- [15] Montserrat Manubens, Didier Devaurs, Lluís Ros, and Juan Cortés. Motion planning for 6-d manipulation with aerial towed-cable systems. In *Robotics: science and systems (RSS)*, page 8p, 2013.
- [16] Carlo Masone, Heinrich H Bühlhoff, and Paolo Stegagno. Cooperative transportation of a payload using quadrotors: A reconfigurable cable-driven parallel robot. In *Proc. IEEE/RSJ Int. Conf. Intell. Robots Syst.*, pages 1623–1630, 2016.
- [17] Daniel Mellinger and Vijay Kumar. Minimum snap trajectory generation and control for quadrotors. In *Proc. IEEE Int. Conf. Robot. Autom.*, pages 2520–2525. IEEE, 2011.
- [18] Gabriele Nava, Quentin Sablé, Marco Tognon, Daniele Pucci, and Antonio Franchi. Direct force feedback control and online multi-task optimization for aerial manipulators. *IEEE Robotics and Automation Letters*, 5(2):331–338, 2019.
- [19] Pedro O Pereira and Dimos V Dimarogonas. Control framework for slung load transportation with two aerial vehicles. In *Proc. IEEE Conf. Decis. Control*, pages 4254–4259, 2017.
- [20] load with a team of uavs. In *2020 International Conference on Unmanned Aircraft Systems (ICUAS)*, pages 158–165. IEEE, 2020.
- [21] James A Preiss, Wolfgang Hönig, Gaurav S Sukhatme, and Nora Ayanian. Crazyswarm: A large nano-quadcopter swarm. In *Proc. IEEE Int. Conf. Robot. Autom.*, pages 3299–3304, 2017.
- [22] Damien Six, Sébastien Briot, Abdelhamid Chriette, and Philippe Martinet. The kinematics, dynamics and control of a flying parallel robot with three quadrotors. *IEEE Trans. Robot. Autom. Lett.*, 3(1):559–566, 2017.
- [23] B. Stellato, G. Banjac, P. Goulart, A. Bemporad, and S. Boyd. OSQP: an operator splitting solver for quadratic programs. *Mathematical Programming Computation*, 12(4):637–672, 2020.
- [24] Sihao Sun and Antonio Franchi. Nonlinear mpc for full-pose manipulation of a cable-suspended load using multiple uavs. *arXiv preprint arXiv:2301.08545*, 2023.
- [25] Andrea Tagliabue, Mina Kamel, Roland Siegwart, and Juan Nieto. Robust collaborative object transportation using multiple mavs. *I. J. Robotics Res.*, 38(9):1020–1044, 2019.
- [26] Marco Tognon, Chiara Gabellieri, Lucia Pallottino, and Antonio Franchi. Aerial co-manipulation with cables: The role of internal force for equilibria, stability, and passivity. *IEEE Trans. Robot. Autom. Lett.*, 3(3):2577–2583, 2018.
- [27] Elio Tuci, Muhanad HM Alkilabi, and Otar Akanyeti. Cooperative object transport in multi-robot systems: A review of the state-of-the-art. *Frontiers in Robotics and AI*, 5:59, 2018.